Journal of Structural Geology 32 (2010) 1873–1886

Contents lists available at ScienceDirect

Journal of Structural Geology

journal homepage: www.elsevier.com/locate/jsg

Pure and shear-enhanced compaction bands in Aztec Sandstone

Peter Eichhubl*, John N. Hooker, Stephen E. Laubach

Bureau of Economic Geology, Jackson School of Geosciences, The University of Texas at Austin, TX 78758, USA

ARTICLE INFO

Article history:
Received 1 September 2009
Received in revised form
11 February 2010
Accepted 17 February 2010
Available online 26 February 2010

Keywords:
Sandstone
Compaction
Deformation band
Localization
Aztec sandstone

ABSTRACT

We report on the occurrence of deformation bands in Jurassic eolian Aztec Sandstone at Valley of Fire, Nevada, that accommodated roughly equal amounts of shear and band-perpendicular compaction by grain rearrangement and porosity collapse. These bands, referred to as shear-enhanced compaction bands, differ in orientation, structural arrangement, and microtexture from pure compaction bands that form perpendicular to the shortening direction. Shear-enhanced compaction bands are planar over tens of meters, and commonly composed of multiple parallel thinner strands. Pure compaction bands are less commonly planar, typically wavy or chevron in geometry, and composed of single strands. Shear-enhanced compaction bands are inferred to form at 38–53° relative to the maximum compressive principal stress, and thus differ from compactive shear bands that form at distinctly lower angles. While shear offsets along shear-enhanced compaction bands are only about 1/10th of the band thickness, by contrast, shear offsets may be large for compactive shear bands with formation of slip surfaces. Based on inferred timing and burial conditions, we interpret that the formation of shear-enhanced and pure compaction bands requires large initial porosity close to the loose packing porosity, good sorting, and high effective maximum compressive principal stress of about 20 MPa.

1. Introduction

Deformation localization in sediment and porous sedimentary rock has received increasing attention in recent years, providing insights into localization processes in geologic systems in general (Bésuelle and Rudnicki, 2004; Aydin et al., 2006; Fossen et al., 2007). Building on an earlier conceptional framework by Houlsby and Wroth (1980), Aydin et al. (2006) distinguished two fundamental modes of deformation localization: (1) Sharp modes of deformation localization are formally defined by a discontinuity in the displacement field and result in opening-mode fractures or joints, and slip surfaces. (2) Tabular modes of deformation localization are zones of finite width bound by two roughly parallel surfaces defined as discontinuities in the displacement gradient field. Deformation bands are a natural expression of the tabular mode of deformation localization. We use the term deformation band to include shear bands, compaction bands, and dilation bands based on the dominant component in displacement gradient across the band relative to the band orientation (sensu Du Bernard et al., 2002; Aydin et al., 2006). Based on theory and the observation that shear bands curve into both compaction and dilation bands, deformation bands may develop at 0° through 90° to the shortening direction, involving appropriate combinations of shear, dilation and compaction (Mollema and Antonellini, 1996; Rudnicki and Olsson, 1998; Issen and Rudnicki, 2000; Bésuelle, 2001; Du Bernard et al., 2002; Borja and Aydin, 2004; Aydin et al., 2006; Fossen et al., 2007). Pure compaction bands are oriented perpendicular to the maximum principal shortening direction, and pure dilation bands perpendicular to the least principal shortening direction within a five-fold division that includes pure compaction bands, compactive shear bands, isochoric shear bands, dilatant shear bands, and pure dilation bands.

Despite the attention compaction localization has received in the engineering disciplines, field descriptions of compaction bands formed under geologic conditions are few. A description of compaction bands was first provided by Hill (1989) in Aztec Sandstone at Valley of Fire, Nevada. Later descriptions include those by Mollema and Antonellini (1996) and Schultz (2009) from the East Kaibab monocline, Utah, and by Sternlof et al. (2004), Holcomb et al. (2007), and Aydin and Ahmadov (2009) from Valley of Fire. However, different authors designated different sets of deformation bands as compaction bands. Sternlof et al. (2004) and Holcomb et al. (2007) designated bands as compaction bands that are oblique relative to the maximum principal shortening direction as inferred by Hill (1989). The compaction bands of Sternlof et al. (2004) and Holcomb et al. (2007) are at high angle to the bedding-parallel compaction bands described by Aydin and Ahmadov (2009). Mollema and Antonellini (1996) described two

* Corresponding author. Tel.: +1 512 475 8829.
E-mail address: peter.eichhubl@beg.utexas.edu (P. Eichhubl).

0191-8141/$ – see front matter © 2010 Elsevier Ltd. All rights reserved.
doi:10.1016/j.jsg.2010.02.004

sets of compaction bands occurring side-by-side from the East Kaibab monocline with same strike but 20° difference in dip angle.

This study was designed to (1) describe the field relationships of compaction and shear bands at Valley of Fire, (2) describe their microstructural characteristics, and (3) place them in a mechanical framework. We will demonstrate that planar pure compaction bands, oriented perpendicular to the direction of maximum principal shortening, form under specific loading conditions, providing a possible explanation why compaction bands have thus far been reported from only two field locations. In addition, we demonstrate that shear-enhanced compaction bands, observed previously in experiment (Fortin et al., 2006; Baud et al., 2006), occur as a distinct type of deformation bands which differ in orientation, textural properties, and geometric relations from pure compaction bands and compactive shear bands.

2. Field structural characteristics of deformation bands

Deformation bands at Valley of Fire are most abundant in the upper section of the Jurassic Aztec Sandstone and the lower section of the Cretaceous Baseline Sandstone (Fig. 1). The Aztec Sandstone is a well-sorted, cross-bedded, and medium-grained sandstone deposited in a backarc setting (Marzolf, 1990). The Baseline Sandstone is a syntectonic molasse sequence of sandstone and conglomerate deposited in front of the Sevier thrust complex (Aschoff and Schmitt, 2008). Our detailed field descriptions of deformation bands focus on the Aztec Sandstone with a more uniform lithology than the Baseline Sandstone. Deformation bands are readily observed in outcrop due to their higher resistance to erosion resulting in positive relief of the bands. The upper section of the Aztec Sandstone is generally weakly cemented, increasing in induration toward its base. In addition to their positive relief, the observation of deformation bands in the upper Aztec Sandstone is aided by the preferred dissolution and reprecipitation of diagenetic iron oxides and hydroxides along bands (Eichhubl et al., 2004).

Deformation bands in the Aztec Sandstone exhibit large variations in band thickness, band spacing, slip amount, orientation, geometric properties, and microtextural properties. Band thickness ranges from ~1 mm to >5 cm, with bands thicker than ~1 cm typically composed of multiple parallel strands. Band spacing ranges from ~5 mm to > 1 m, and slip from 0 to >10 cm.

Structural cross-cutting relations indicate three stages of deformation band formation. Stage I are Late Cretaceous in age based on cross-cutting relations with Sevier-age thrust faults (Eichhubl and Flodin, 2005) and are the focus of this study. Stage I deformation bands occur in eight sets that differ in orientation, structural style, and microtexture (Table 1). Set 1 consists of bands with no discernible shear, which we interpret to be pure compaction bands. Sets 2–6 are bands with discernible slip of ~1/10th band thickness, which we define as shear-enhanced compaction bands. Sets 7 and 8 are bands with slip that typically exceeds the band thickness; while they are compactive shear bands we refer to them as shear bands for simplicity.

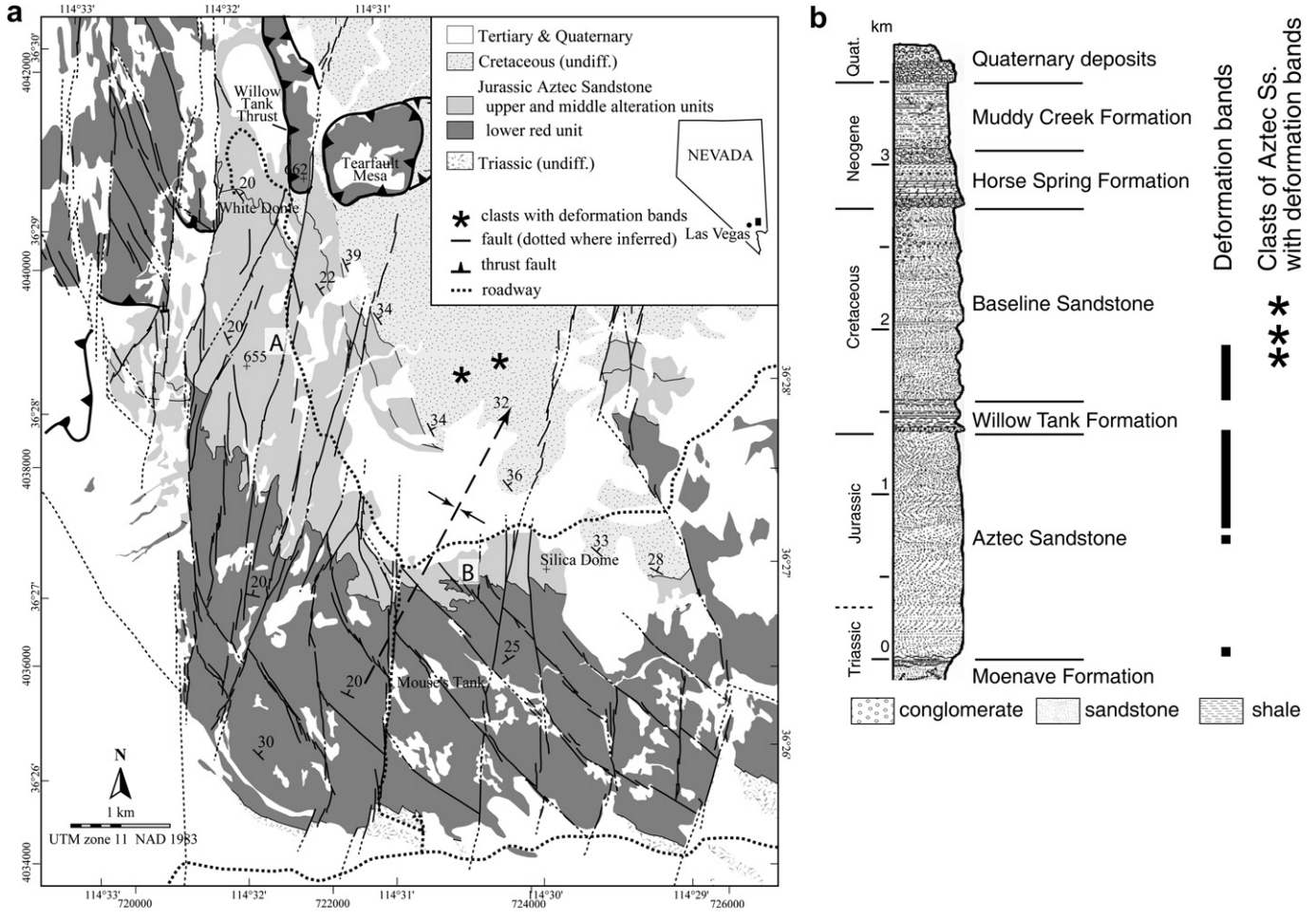

Fig. 1. a. Geologic map of Valley of Fire, after Eichhubl et al. (2004). b. Stratigraphic column of Valley of Fire after Bohannon (1977).

Table 1
Stage I deformation bands in upper Aztec Sandstone at Valley of Fire.

Set	1	2	3	4	5	6	7	8
Mode	Pure compaction	Shear-enhanced compaction	Shear-enhanced compaction	Shear-enhanced compaction	Shear-enhanced compaction	Shear-enhanced compaction	Compactive shear	Compactive shear
Relative orientation	High-angle to bedding	Reverse	Reverse	Left-lateral strike-slip	Right-lateral strike-slip	Bedding-parallel	Bedding-parallel	Reverse
Strike, dip	N20°E, 26°W	N8°W, 24°E	N70°E, 28°N	N61°E, 20°N	N15°W, 9°W	N85°E, 17°N	N85°E, 17°N	N26°W, 44°E
Structural style	Wavy, rarely planar	Planar	Planar	Planar or chevron	Planar or chevron	Planar, ramp-flat	Planar	Planar
Microtexture	Minor cataclasis	Minor cataclasis	Minor cataclasis	Minor cataclasis	Minor cataclasis	Minor cataclasis	Strong cataclasis	Strong cataclasis
Force chains[a]	Poorly coordinated	Well coordinated	Well coordinated	Well coordinated	Well coordinated			

[a] See Section 3.2.1 for explanation.

Stage I shear-enhanced compaction bands are the most ubiquitous brittle structures in the upper Aztec Sandstone. They are planar to curviplanar, and can be traced over 10–50 m along strike (Fig. 2a). Bands are up to 5 cm thick, and composed of up to 10–20 single strands. Where suitable markers are available, offset along these bands are about 1 mm for bands of 1 cm thickness (Fig. 2b). Shear-enhanced compaction bands occur in five sets: Two conjugate sets (sets 2 and 3, Table 1) strike about N8°W and N70°E, respectively, (Fig. 3) with a reverse sense of slip based on offset bedding laminae (Fig. 2b). Two other conjugate sets strike NE (set 4, N061°E) and NNW (set 5, N15°W) with a strike-slip sense. Due to the lack of outcrop-scale markers, the strike-slip sense is commonly not observable in the field but inferred from microtextural characteristics. A fifth set of shear-enhanced compaction bands (set 6) is oriented parallel to bedding (Fig. 2c) (Eichhubl, 2007; Aydin and Ahmadov, 2009). Bedding-parallel shear-enhanced compaction bands tend to ramp up or down across bedding (arrows in Fig. 2c). Within those ramps, bedding laminae cut across the bands, indicating that these bands are structural features and not depositional in origin.

Two sets of shear bands are associated with the first stage of deformation band formation. One set (set 7, Table 1) occurs as bedding-parallel bands in the more clay-rich bottom sets of dune sets (Fig. 2d). Sense of slip is generally top to the east. Bedding-parallel shear bands are 1–2 mm thick, have 1–2 cm of slip, and can be followed across large dunes sets for >20 m along strike. A second set of shear bands (set 8) is oriented at large angle to bedding with a mean orientation of N26°W, 44°E. Shear bands of set 8 generally form a set of distinct orientation with a lesser dip angle than adjacent reverse-slip shear-enhanced compaction bands (Fig. 2e). Locally, however, shear bands of set 8 turn parallel to, and follow, reverse-slip shear-enhanced compaction bands (dashed line in Fig. 2e). We interpret this change in direction of shear bands in the vicinity of shear-enhanced compaction bands to indicate that the shear bands formed after the shear-enhanced compaction bands. Single shear bands are less than 5 mm in thickness but may form bundles of multiple parallel bands of 1–2 cm in thickness and 1–2 cm of reverse-slip (Fig. 2f). Shear bands parallel to bedding (set 7) and at high angle to bedding (set 8) mutually offset indicating that they formed concurrently.

Pure compaction bands form a single set (set 1) of strike N020°E, dip 26°W, bisecting the acute 80–90° angle between left- and right-lateral strike-slip shear-enhanced compaction bands (sets 4 and 5) (Fig. 3). Pure compaction bands are rarely planar but characteristically wavy (Fig. 4a); they frequently transition along strike into a zigzag or chevron pattern of alternating left- and right-lateral shear-enhanced compaction bands with sharp ~90–100° corners and planar "limbs" (Fig. 4b). This chevron pattern is commonly fairly regular, maintaining a constant wavelength and amplitude over several meters along strike. The average strike of these regular chevron-type bands is parallel to planar or wavy pure compaction bands (set 1), with individual limbs of the chevron structure being aligned parallel to sets 4 and 5. In other cases, chevron-type bands are composed of limbs of varying length, or regular chevron-type bands lose their regularity and continue as planar shear-enhanced compaction bands for tens of meters (Figs. 4c and 5). Thus, planar or wavy pure compaction bands can continue along strike as regular or irregular chevron-type compaction bands, and chevron-type bands can continue as planar shear-enhanced compaction bands. Mutual cross-cutting relations are observed among pure and shear-enhanced compaction bands (sets 2–5) indicating that pure compaction bands and planar or chevron-type shear-enhanced compaction bands formed concurrently. We have no evidence that compaction bands consistently initiated as either pure or shear-enhanced compaction bands that later evolved into shear-enhanced or pure compaction bands, respectively, with continued growth or propagation. The presence of mutual cross-cutting relationships suggests that band initiation can occur as either pure and shear-enhanced compaction bands.

A large pavement of shear-enhanced strike-slip compaction bands and wavy to chevron-type pure compaction bands was mapped by Hill (1989) (Fig. 5a). He observed that bands in the set 1 direction (wavy compaction bands and regular chevron-type bands) are more abundant in this outcrop than planar shear-enhanced compaction bands (sets 4 and 5). Assuming that all sets of bands accommodated roughly equal amounts of shortening perpendicular to their mean strike direction he inferred that bands in the set 1 direction are perpendicular to the outcrop-scale maximum principal shortening direction, and that sets 4 and 5 are oriented at 45–50° to the maximum shortening direction. Microtextural observations presented below confirm his assumption and interpretation.

The spacing between wavy and chevron-type compaction bands ranges from <1 cm to >1 m, with equally spaced sets of 5–10 cm spacing being common (Fig. 4a, b). Where chevron-type compaction bands are closely spaced we observe that the "crests" and "troughs" of neighboring bands are in some cases parallel or "in phase". More commonly, however, the crests and troughs of neighboring bands are "out-of-phase" (Fig. 4d). This geometry suggests that adjacent chevron-type bands do not affect each other's turning behavior. The lack of coordination among neighboring bands also suggests that the switch in direction of chevron-type bands reflects stress and strain boundary conditions in the immediate vicinity of a band.

Pure and shear-enhanced compaction bands and shear bands occur within specific parts of a dune set (Fig. 6): Foresets contain pure compaction bands (set 1), two sets of strike-slip shear-enhanced compaction bands (sets 4 and 5) as mapped by Hill (1989), and bedding-parallel shear-enhanced compaction bands (set 6). Bedding-parallel shear bands are typically absent. Bottom

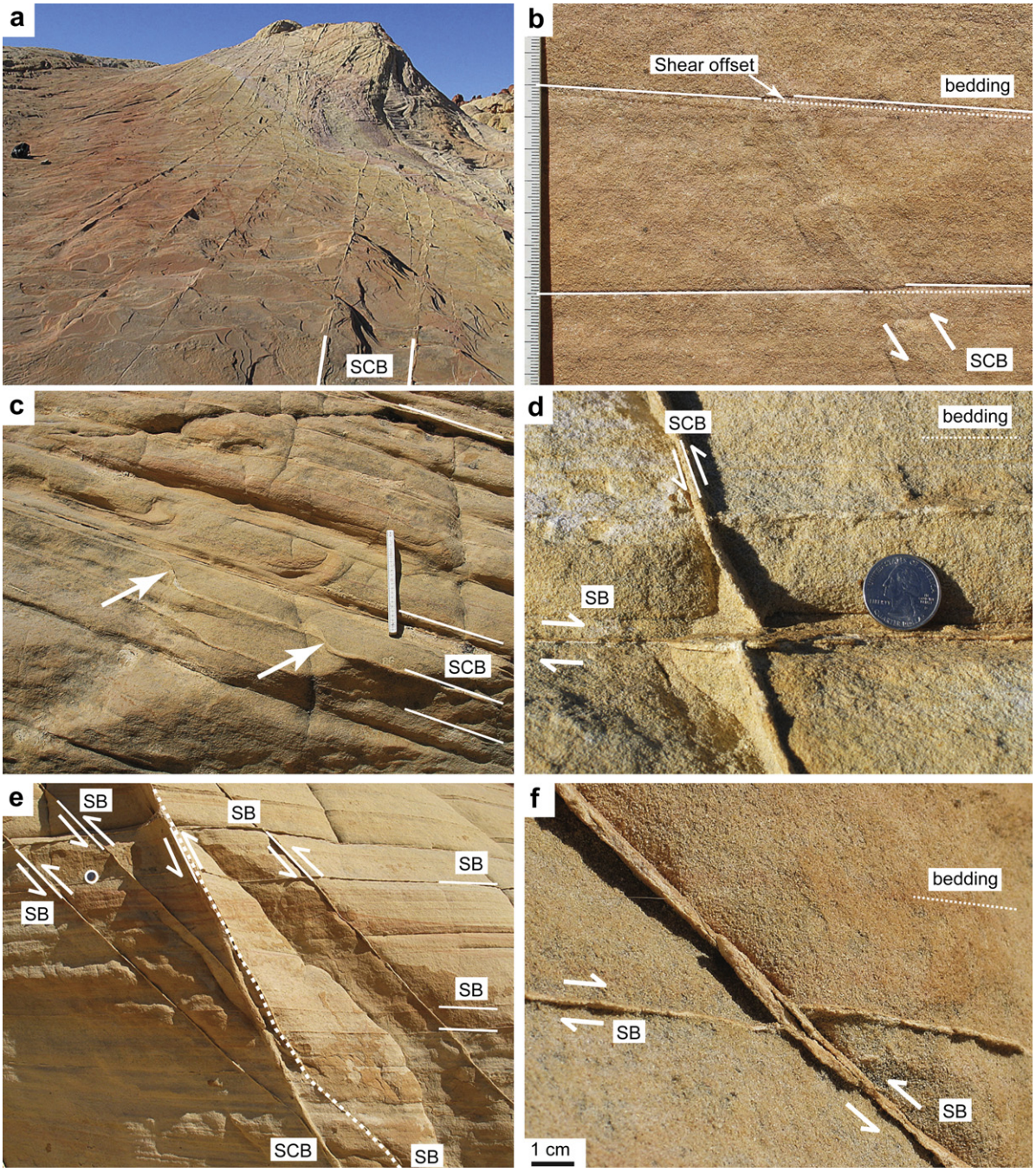

Fig. 2. Shear-enhanced compaction bands (SCB) and shear bands (SB) in Aztec Sandstone. a. Set of planar shear-enhanced compaction bands on bedding surface. Spacing between highlighted bands in foreground about 40 cm b. Shear-enhanced compaction bands with ~1 mm of reverse-slip viewed across bedding. Large divisions on scale are centimeters. c. Bedding-parallel shear-enhanced compaction band. Note flat-ramp-flat geometry of band, with ramp segment cutting across bedding (arrows). d. Bedding-parallel shear band with 1 cm offset. e. Shear-enhanced compaction bands and shear bands viewed across bedding. Coin (top left circled) for scale. Dashed line highlights the turning of shear bands into parallelism with shear-enhanced compaction bands. f. Reverse-slip shear band at high angle to bedding with ~1 cm or reverse-slip, offsetting bedding-parallel shear band.

sets contain two sets of reverse-slip shear-enhanced compaction bands (sets 2 and 3) and bedding-parallel shear bands (set 7). Pure compaction bands and strike-slip shear-enhanced compaction bands were not observed in bottom sets. The exclusive occurrence of pure compaction bands in the absence of bedding-parallel shear bands suggests that bedding-parallel shear suppresses the formation of pure compaction bands.

The change in band orientation from foreset to bottom set can be abrupt or gradual (Figs. 6 and 7). Reverse-slip shear-enhanced compaction bands in bottom sets change into straight or chevron-type strike-slip shear-enhanced compaction bands as the bands cross into foreset layers over a distance of 1–10 cm. Pure compaction bands in foresets either terminate or continue into the bottom set as reverse-slip shear-enhanced compaction bands. Changes in band orientation and style are also observed at dune boundaries. Where a dune boundary overlies an eroded foreset, the majority of pure compaction bands in the foreset terminates against the dune boundary with a small number continuing as reverse-slip shear-enhanced compaction bands into the bottom set of the overlying dune set. Where the dune boundary overlies an eroded and

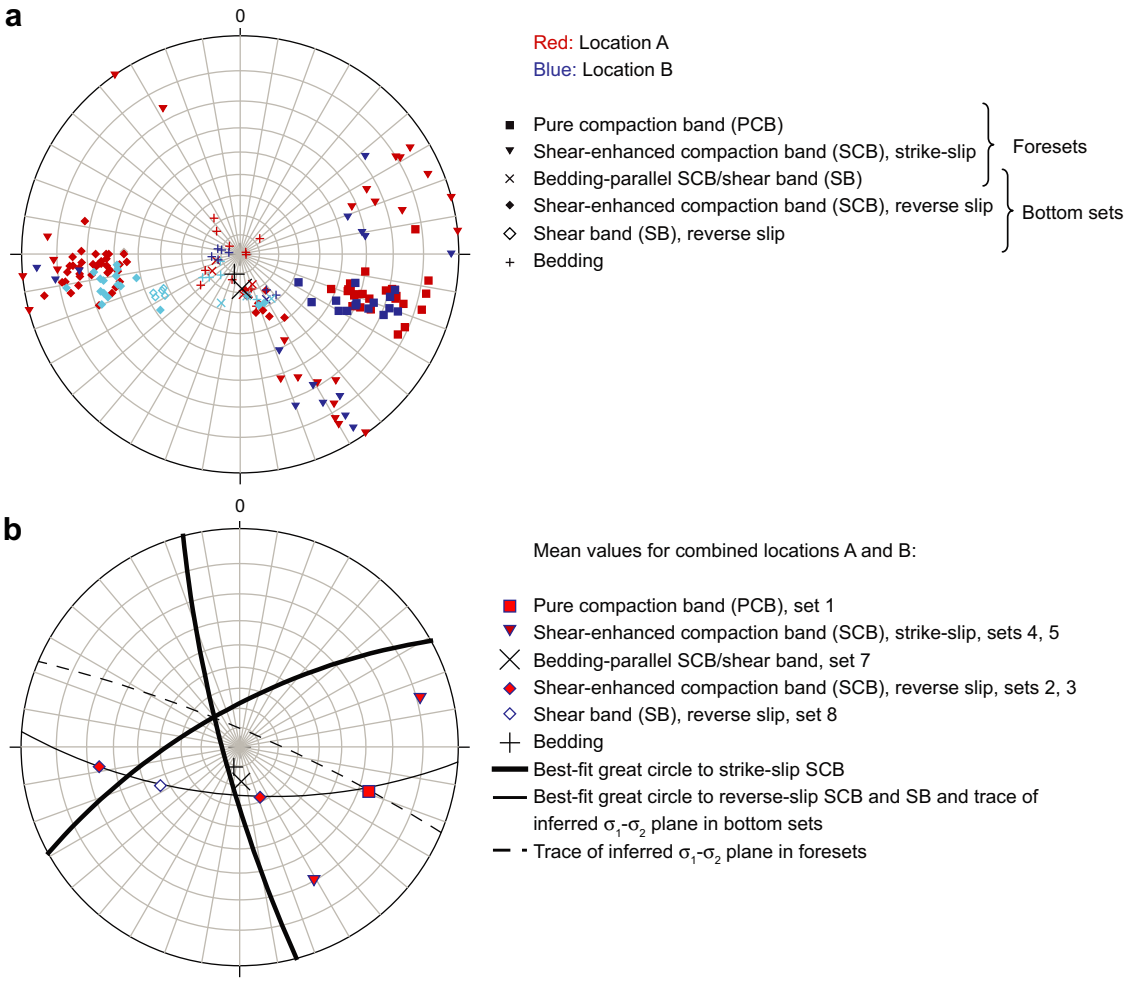

Fig. 3. a. Orientation of deformation bands and bedding planes for locations A and B at Valley of Fire. Wulff net (equal angle), lower hemisphere projection. b. Mean values and interpretation.

truncated bottom set (Fig. 6), bedding-parallel shear bands and shear-enhanced compaction bands continue as reverse-slip shear-enhanced compaction bands into the overlying bottom set provided the bedding orientation of the truncated dune set is suitably oriented.

3. Textural characteristics

3.1. Methods

Oriented hand samples of deformation bands were vacuum impregnated with blue-dyed epoxy prior to cutting to avoid grain plucking during thin section preparation. Trimmed samples were impregnated a second time to achieve complete blue-epoxy impregnation. Polished sections were imaged petrographically, by scanning-electron microscope (SEM)-backscatter electron (BSE) imaging, and using SEM-based color cathodoluminescence (CL). SEM imaging was performed on a Siemens XL30 SEM equipped with an Oxford Mono-CL detector, outfitted with a color-filter array for consecutive blue-, green-, and red-channel image acquisition. Single-channel images were stacked into RGB images using NIH ImageJ. Sections were imaged at 150× nominal magnification, with multiple images mosaicked in Adobe Photoshop. Point counting of detrital grain composition, pore space, and quartz cement abundance was performed on stacked color-CL, electron backscatter, and optical microscope images using the software JMicroVision (Table 2).

3.2. Results

Aztec Sandstone is compositionally and texturally mature, composed of, on average, 96% quartz grains and 3% feldspar (relative to 100% detrital grains). The sandstone has an average porosity of 18% and contains 3% quartz cement and 3% clay cement. Grains are well rounded, and grain sizes well sorted, although mean grain size varies between fine and coarse sand among laminae. Outside deformation bands, sand grains tend to be indented at grain-to-grain contacts, resulting in concavo-convex contacts (Fig. 8a). Grain indentation is accompanied by intragranular and less common intergranular microfractures. Microfractures radiate out from grain contacts. SEM-CL at high magnification of grain contacts reveals that grain indentation is the result of both chemical and mechanical processes. While quartz overgrowth cement on quartz grain surfaces is absent in the upper Aztec Sandstone, quartz cement is contained in microfractures both within and outside deformation bands. We attribute the preferred quartz cementation in microfractures to the preference of quartz to precipitate on a quartz substrate that is free of clay and iron oxide coats.

3.2.1. Pure and shear-enhanced compaction bands

All types of stage I deformation bands are characterized by a reduction in porosity relative to the adjacent host sandstone (Table 2). The difference in porosity between host and band ranges between 4 and 11% for pure and shear-enhanced compaction

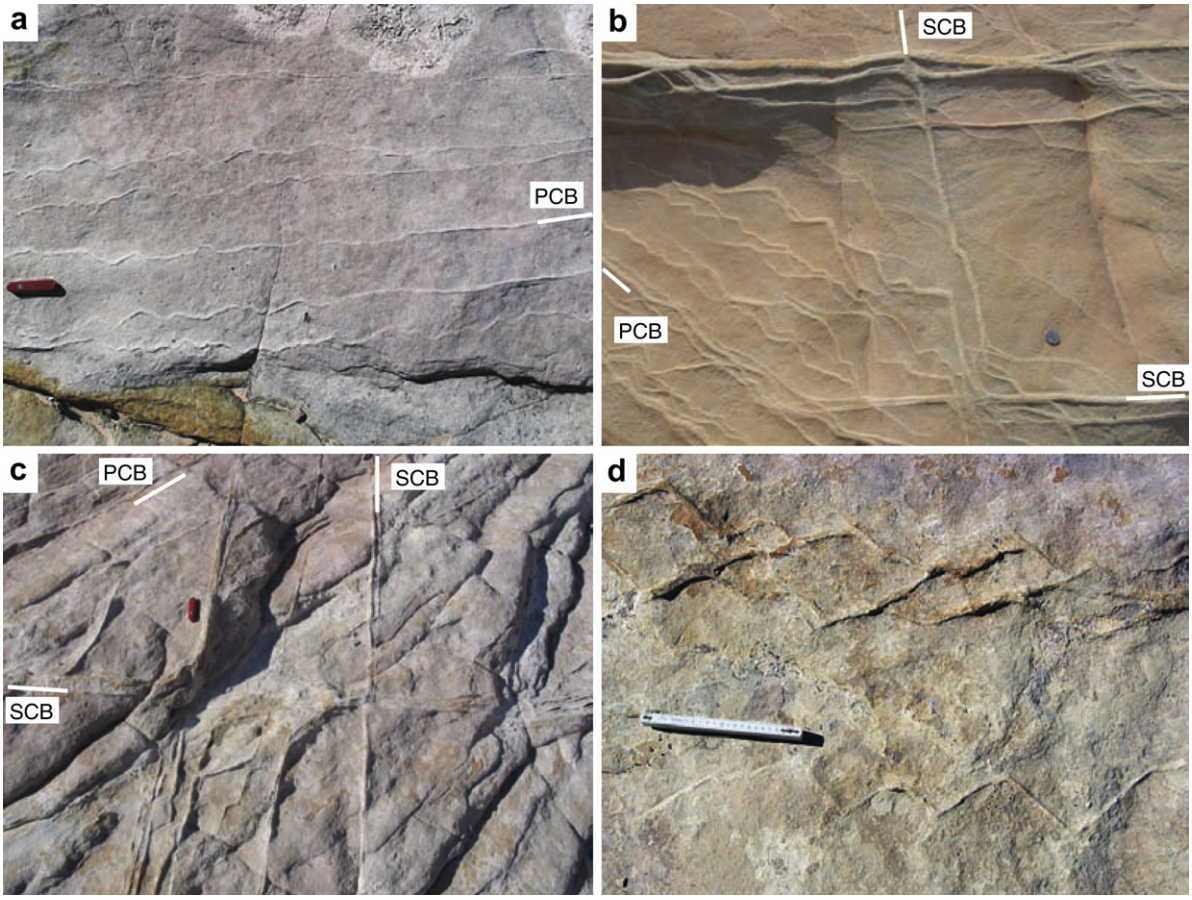

Fig. 4. Pure (PCB) and shear-enhanced (SCB) compaction bands exposed on a bedding plane. a Pure compaction bands with characteristic wavy trace. Pocket knife for scale. b. Chevron pattern of alternating right- and left-lateral shear-enhanced compaction bands. Chevron-style bands merge with and continue as planar shear-enhanced compaction bands. c. Intersection of sets of shear-enhanced compaction bands. d. Chevron-type compaction bands with out-of-phase alignment of crests and troughs.

bands. Part of this porosity reduction results from enhanced precipitation of quartz cement in deformation bands, ranging between 5 and 7%. Differences in intergranular volume (IGV), ranging from −1 to 8%, take quartz cementation into account and are therefore a better estimate of mechanical porosity reduction associated with the formation of deformation bands. The negative IGV value may reflect quartz cement formed during deformation, or detrital quartz cement that predates deposition.

While amounts of porosity reduction and cementation are similar for pure and shear-enhanced compaction bands, we observe distinct differences in microtextural ordering. The degree of microtextural ordering inside and outside deformation bands, and between pure and shear-enhanced compaction bands, was determined by the preferred orientation and trace length of chains composed of grains that are in concave-convex contact (Fig. 8). Trajectories of these chains were observed and mapped in backscatter (BES) and cathodoluminescence (CL) SEM images by connecting adjacent grains with concave-convex contacts. Trajectories were then constructed for a minimum of three contacting grains, perpendicular to the grain contacts (red lines in Fig. 8b, c), and parallel to microfractures that radiate away from grain-to-grain contacts (blue lines in Fig. 8b, c). We refer to these trajectories as force chains (Oda et al., 1982; Potyondy and Cundall, 2004) and consider them a two-dimensional proxy for the orientation of the load-bearing framework in the three-dimensional granular aggregate. Force chains were mapped on thin sections cut perpendicular to the band, thus containing the direction of maximum principal shortening (Figs. 8c and 9). For shear-enhanced compaction bands, thin sections were also oriented parallel to the slip vector as observed as shear offset in outcrop or inferred based on their conjugate geometry and orientation relative to pure compaction bands (Figs. 3, 8c and 9a).

In a well sorted sample, force chains span over 10 grains (Fig. 8). Force chains are best developed, and most easily recognized, in well sorted sandstone with grain breakage limited to grain contacts and with a minimum of fine-grained matrix. Force chains are less well defined with decrease in sorting and an increasing amount of matrix or crushed grains.

Based on the preferred orientation and trace length, force chains in shear-enhanced compaction bands are longer and have stronger modal attitudes than force chains in pure compaction bands (Figs. 8–10). In shear-enhanced compaction bands, force chains are well defined, with a preferred orientation at around 45° relative to the band orientation (Fig. 10b and c). For the strike-slip shear-enhanced compaction band (Figs. 9a and 10b), this orientation is approximately parallel to the direction of outcrop-scale maximum principal shortening as inferred based on the dihedral angles of 106° between the conjugate sets 4 and 5. For the pure compaction band in Fig. 9b, force chains are less well defined, with shorter chain lengths and a weakly defined preferred orientation (Fig. 10c).

3.2.2. Shear bands

In shear-enhanced compaction bands, microfractures are limited largely to grain-to-grain contacts as the majority of grains retain their detrital shape and provide the load-supporting framework. In contrast, the majority of grains in shear bands have

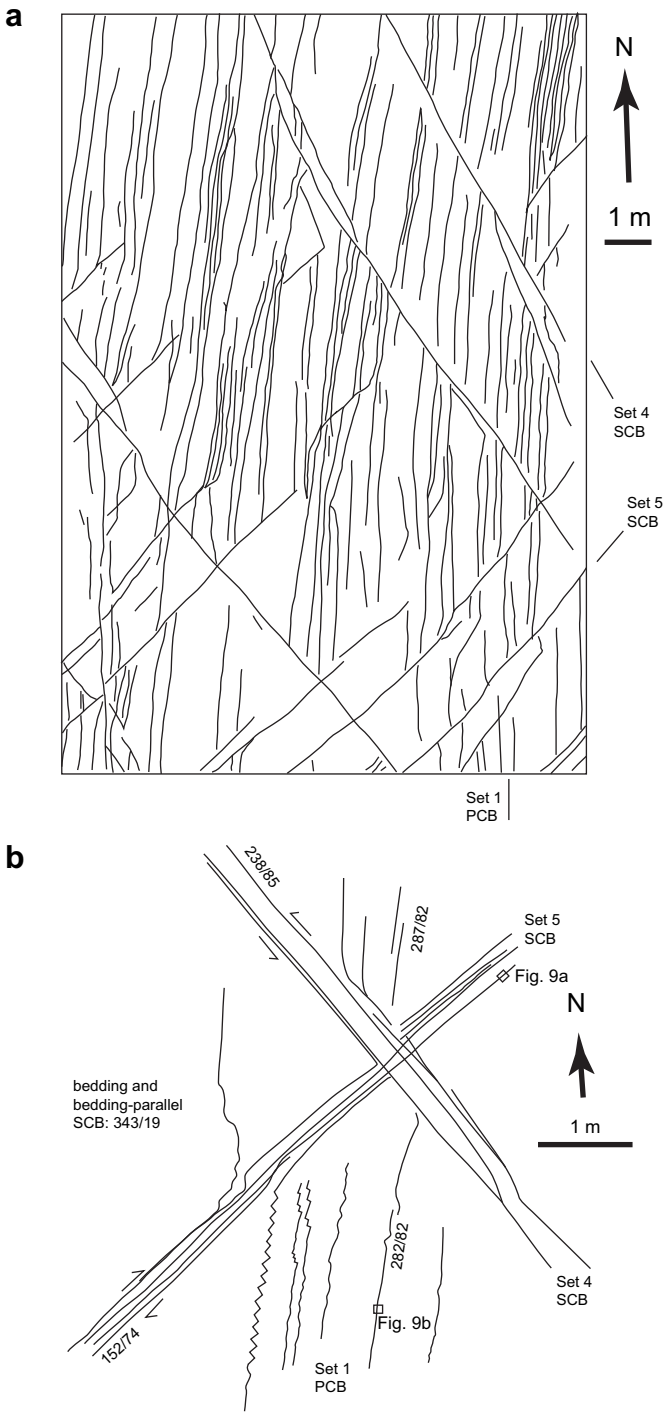

Fig. 5. a. Pavement of pure and strike-slip shear-enhanced compaction bands. After Hill (1989). Location A in Fig. 1. b. Outcrop sketch of wavy pure compaction bands and strike-slip shear-enhanced compaction bands as observed on bedding surface. Pure compaction bands turn into chevron patterns of alternating left- and right-lateral shear-enhanced compaction bands, and straight shear-enhanced compaction bands, and vice versa. Sense of shear is based on microtextural observations (Fig. 9a). Orientations given as dip azimuth, dip. Location A in Fig. 1.

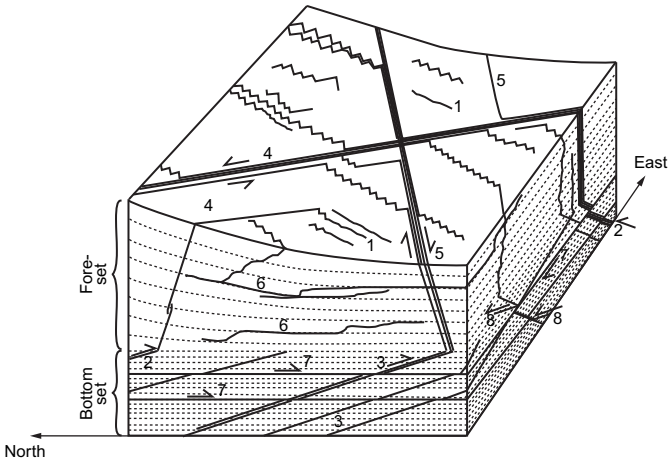

Fig. 6. Diagram about distribution of pure and shear-enhanced compaction bands at Valley of Fire as a function of position within dune sets. Numbers refer to sets of deformation bands in Table 1.

undergone significant grain-size reduction (Fig. 11). SEM-CL imaging of shear bands (Fig. 11a) reveals that the bands are composed of an outer zone (dashed in Fig. 11a) of grain crushing and pore collapse but limited shear, and an inner ~200 μm wide zone of concentrated slip. This zonation compares to the fault damage zone and fault core of macroscopic faults (Caine et al., 1996). While the outer zone contains survivor grains embedded in a matrix of highly fragmented grains, the inner zone shows a high degree of grain-size reduction and no survivor grains. In CL, trails of fragments of individual offset grains can be traced across the inner zone. Although finer cataclastic material appears to be missing from the inner zone, presumably a result of sample handling and preparation, steps in these fragment trails suggest the presence of 3–4 discrete slip surfaces within the shear band. Due to the apparent loss of fines from the inner zone of the shear band, the amount of compaction and porosity loss cannot be quantified. The tight grain packing in the outer zone of the shear band indicates significant pore collapse and compaction across the band, allowing designation of these bands as compactive shear bands. By comparison, shear-enhanced compaction bands lack discernible slip surfaces. In addition, we note that, due to the high degree of cataclasis, force chains cannot be traced within the inner zone of this shear band.

Fig. 11b and c depict a ~7 mm wide stage II compactive shear band with about 1 cm of reverse-slip. Stage II compactive shear bands are narrow (<0.5 cm thick) and occur in ESE-WNW striking zones composed of closely spaced bands that are frequently arranged in ladder geometry. These zones extend over 300 m in length, with similar spacing. Stage II bands crosscut and thus postdate pure and shear-enhanced compaction bands but may overlap in time with stage I compactive shear bands from which they differ in orientation and structural style. Like stage I deformation bands, stage II bands are interpreted to be Late Cretaceous in age.

Compared to the shear band in Fig. 11a, shear in the band of Fig. 11b is more distributed resulting in smaller shear strain and a greater abundance of survivor grains. Although frequently fractured, survivor grains preserve their detrital shape and float in a matrix of grain fragments (Fig. 11c). Cataclasis is most intense along 5–7 narrow zones that parallel the macroscopic shear band suggesting that the macroscopic band is composed of multiple thinner individual bands ~1 mm in width, with interleaved bands of lesser cataclasis (outlined in Fig. 11b with red dashed lines). Similar to the more cataclastic shear band in Fig. 11a, force chains cannot be delineated for the detrital grains in this matrix-supported fabric. The porosity in the shear band in Fig. 11b (sample 11/23-2A) is 4.5% and IGV is 12% (Table 2). Because quartz cement abundance cannot be determined accurately for intensely fragmented quartz, IGV estimates in shear bands are only approximate.

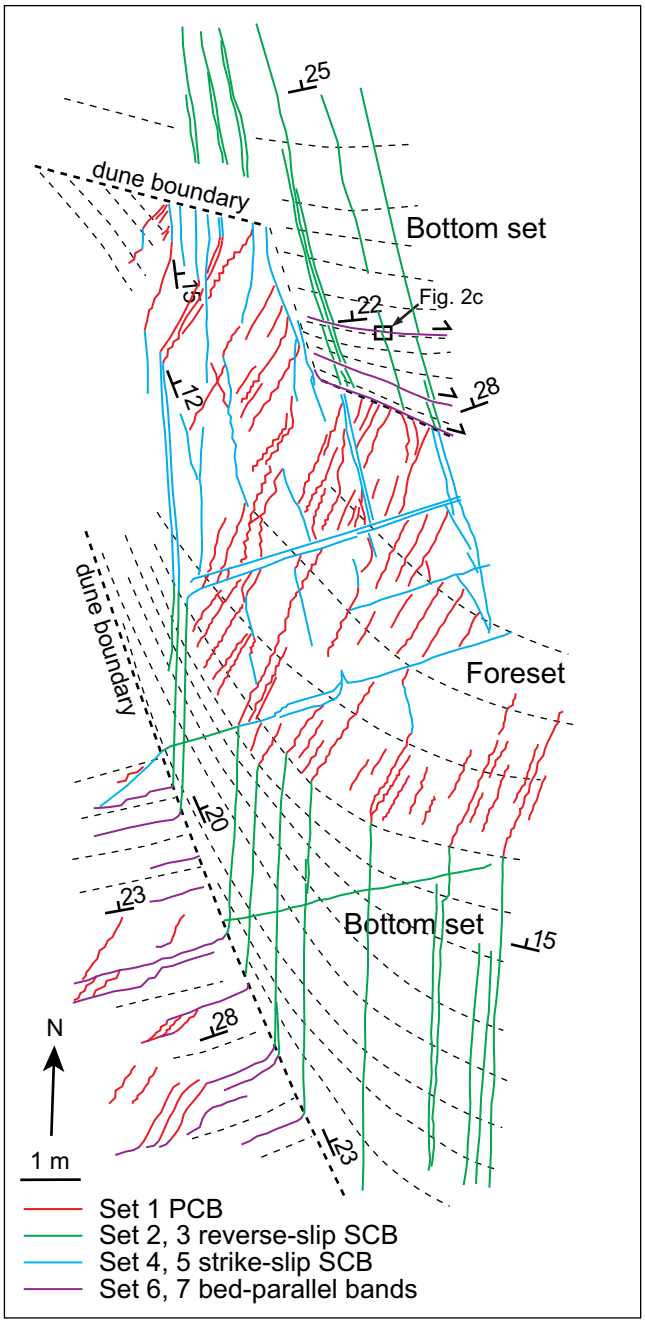

Fig. 7. Map of deformation bands 300 m east of Rainbow Vista (location B in Fig. 1) illustrating change in band orientation across dune boundaries. The apparent offset in the top dune boundary is due to topographic effects.

4. Discussion

4.1. Shear-enhanced compaction bands as distinct structures from pure compaction bands

Shear-enhanced compaction bands differ from pure compaction bands in orientation, microtexture, and, where markers are available, in observed shear offset. The distinct clustering of pure and shear-enhanced compaction band orientations on the stereonet (Fig. 3) is consistent with the field observation that pure and shear-enhanced compaction bands are distinct populations and types of deformation bands. Except for the short distance (<2–3 cm) over which shear-enhanced compaction bands switch between left and right-lateral segments, bands do not assume intermediary orientations between pure and shear-enhanced compaction bands.

For reverse-slip shear-enhanced compaction bands where bedding laminae provide suitable markers (Fig. 2b), the shear component is ~1 mm or about 10% of the thickness of the band. The difference in intergranular volume (IGV) between host rock and band of 8.3% (Table 2) provides an estimate of band-perpendicular shortening of 10% or 1 mm. Band-parallel shear displacement is thus approximately equal to the band-perpendicular shortening displacement with a resultant vector of particle translation oriented 45° to the band. This direction is consistent with the orientation of force chains in shear-enhanced compaction bands (Figs. 8c and 9a). Shear-enhanced compaction bands can thus be regarded as bands that accommodate localized compaction oblique to the loading direction. For strike-slip shear-enhanced compaction bands for which macroscopic markers for shear offset are unavailable, the orientation of force chains at ~45° relative to the band orientation is consistent with oblique shortening across these bands. Shortening perpendicular to pure compaction bands is inferred based on their orientation bisecting conjugate shear-enhanced compaction bands and the lack of macro- or microscopic shear indicators.

In addition, pure and shear-enhanced compaction bands differ in the preferred orientation of force chains. The well developed force chains in shear-enhanced compaction bands suggest that the movement of grains associated with band formation is more ordered than grain movement in pure compaction bands where force chains are oriented more isotropically. While particle movement in response to uniaxial shortening is expected to occur, statistically, parallel to the shortening direction, grain-to-grain collisions will result in a lesser component of particle movement orthogonal to the loading direction. We hypothesize that the preferred orientation of force chains reflects the coordination in the orthogonal movement among neighboring grains. The better developed force chains and the higher degree of textural order in shear-enhanced compaction bands suggest that the shear component of particle flow relative to the macroscopic band orientation favors a well organized particle flow field where the movement of individual grains is coordinated with neighboring grains over distances equal to or larger than the thickness of the band. Short and variously oriented force chains in pure compaction bands, on the other hand, suggest a particle flow field that is heterogeneous and poorly coordinated, with coordination distances that are short relative to the thickness of the band.

4.2. Inferred loading conditions for stage 1 deformation bands

The symmetry between strike-slip shear-enhanced compaction bands and pure compaction bands, in conjunction with the oblique orientation of force chains in shear-enhanced compaction bands, suggests that the pure compaction bands are oriented perpendicular to the maximum compressive principal stress σ_1, bisecting the conjugate set of shear-enhanced compaction bands. For the observed dihedral angle of 106° between the mean orientations of both sets (Figs. 3 and 5), these shear-enhanced compaction bands are thus oriented at about 53° to σ_1. We interpret the uniform orientation of the bands across the study area to reflect the consistent orientation of the regional stress field during band formation, with σ_1 oriented 26/109 (plunge/trend in present coordinates), and the σ_1, σ_2 plane striking NW, dipping steeply NE (dashed line in Fig. 3b). Reverse-slip shear-enhanced compaction bands similarly describe a conjugate set. These bands as well as reverse-slip shear bands, all characteristic of bottom sets, correspond to a 40° rotation of the σ_1, σ_2 plane (thin solid great circle in Fig. 3b) around the inferred regional σ_1 direction. We ascribe this

Table 2
Point-count results of deformation bands and adjacent host rock. For locations see Fig. 1a. Φ: porosity; IGV: intergranular volume; rSCB: reverse-slip shear-enhanced compaction band; ssSCB strike-slip shear-enhanced compaction band; SB: shear band; PCB: pure compaction band; b//: bedding-parallel; bp: bedding-perpendicular.

Sample	Band type	Location Fig. 1	Quartz	Feld spar	Other detrital	Quartz cement	Clay cement	Φ	ΔΦ	IGV	ΔIGV
11/24-4	Host	A	66.5	4.2	2.0	1.2	3.5	22.7	–	27.3	–
11/25-4	PCB	A	76.7	1.5	2.0	4.8	2.8	12.2	10.5	19.8	7.5
11/25-3E	ssSCB	A	72.5	4.2	0.8	6.3	1.8	14.3	8.3	22.5	4.8
11/25-3	Host	B	73.9	1.5	1.0	1.3	6.2	16.1	–	23.6	–
05/25-3	rSCB	B	83.0	0.7	1.0	4.7	4.8	5.8	10.3	15.3	8.3
05/25-1A	Host	B	72.9	0	0.6	3.3	1.5	21.6	–	26.5	–
05/25-1A	b//SCB	B	71.8	0.5	0	7.0	2.7	17.9	3.7	27.6	–1.2
11/25-1A	Host	C	78.4	0.6	0.2	10.0	1.6	9.2	6.8	20.8	–
11/25-1A	rSCB	C	75.9	0.5	1.0	4.8	1.8	16.0	–	22.6	1.8
11/23-2A	Host	D	73.8	5.2	0.2	1.3	1.3	18.2	–	20.8	–
11/23-2A	b//SB	D	76.7	6.5	0.3	5.7	4.8	6.0	12.2	16.5	4.3
11/23-2A	bp SB	D	84.3	3.7	0.5	4.7	2.3	4.5	13.7	11.5	9.3

rotation of the σ_1 σ_2 plane between foresets and bottom sets to bedding-parallel slip and a resultant rotation of the stress tensor in the bottom sets relative to the more homogeneous and mechanically isotropic foresets. The observed dihedral angle between the two sets of reverse-slip shear-enhanced compaction bands in the σ_1 direction is 75°, with the two sets oriented at 33° and 41° to the inferred regional σ_1 direction. Both bands would be bisected at 38° by a σ_1 direction of 24/106, which is indistinguishable from the

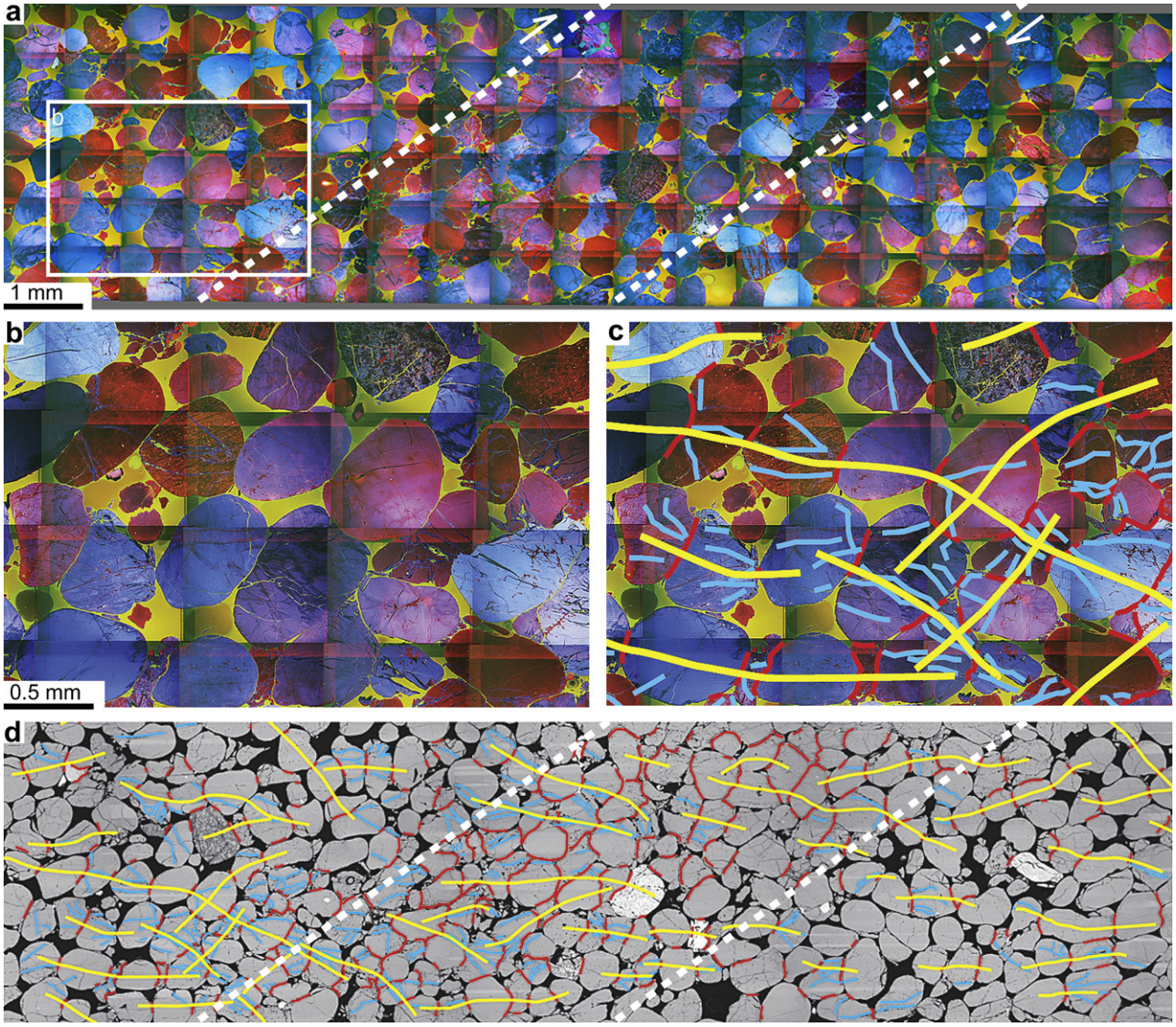

Fig. 8. a. SEM-cathodoluminescence image mosaic of shear-enhanced compaction band with reverse-slip sense of shear. Thin section orientation is vertical. Outline of band is dashed. b. Detail of a. Note brittle deformation along concave-convex grain contacts. c. Same as b. with concave-convex grain contacts marked in red, microfractures in blue, and interpreted force chains in yellow. d. Force chain map of a. over SEM-backscatter image mosaic. See c. for explanation of line colors.

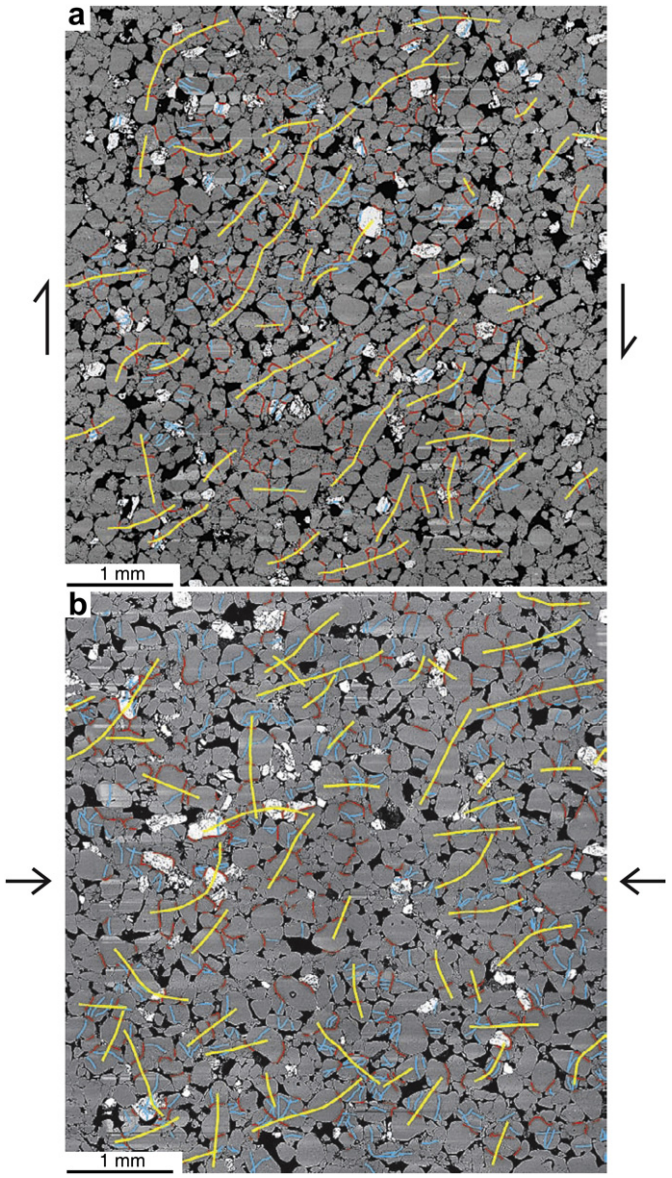

Fig. 9. Force chain maps of a. shear-enhanced compaction band with strike-slip sense of shear, and b. pure compaction band. Note preferred alignment of force chains in shear-enhanced compaction bands compared to pure compaction bands. Images are oriented horizontally and sides of images are parallel to the band boundaries. Arrows indicate inferred shortening direction. See Fig. 5b for relative sample locations and caption of Fig. 8c for explanation of line colors.

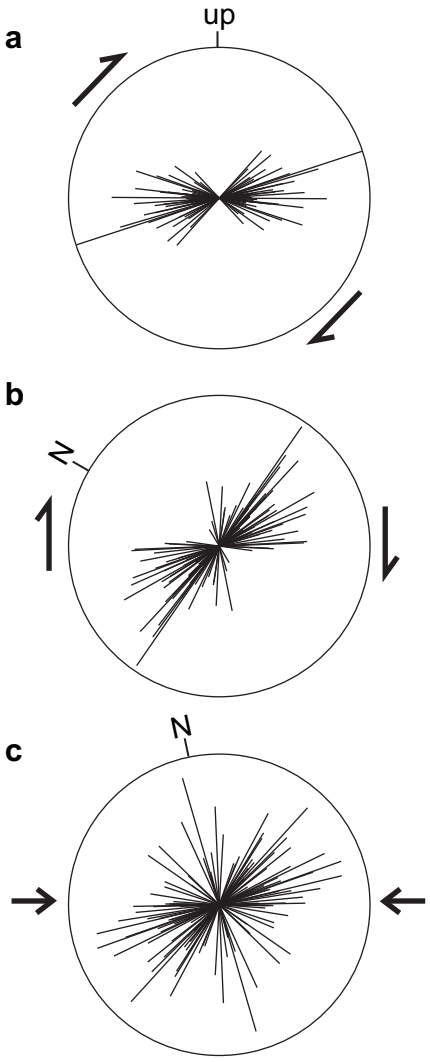

Fig. 10. Directions of force chains mapped in a. Fig. 8, b. Fig. 9a, and c. Fig. 9b. Length of bars is scaled to the length of the longest force chain in each map: a. 5.5 mm; b. 1.4 mm; c. 1.3 mm.

previously determined regional σ_1 direction considering the scatter in band orientations (Fig. 3a). Bedding-parallel and reverse-slip shear bands (sets 7 and 8) are oriented at 32° and 7° relative to the inferred regional σ_1 direction, respectively. For both shear bands to be bisected by σ_1, the σ_1 direction in the bottom sets would be 19/093, or about 10° different in strike from the regional σ_1 direction inferred above for the foresets.

With pure and shear-enhanced compaction bands occurring side-by-side and without consistent cross-cutting relations indicative of sequential formation, we infer that both types of compaction bands formed concurrently under the same regional and outcrop-scale stress conditions. We envision that the switch between pure and shear-enhanced compaction bands, and between right- and left-lateral shear-enhanced compaction bands, is controlled by the local stress field in immediate vicinity of the propagating band. The "out-of-phase" occurrence of adjacent chevron-type bands suggests that the scale of local stress field perturbation is less than the spacing distance between neighboring bands which is on the order of a few centimeters.

The 38°–53° orientation of shear-enhanced compaction bands relative to the inferred direction of the maximum compressive principal stress is similar to the 37°–55° orientation of bands relative to the loading direction observed by Friedman and Logan (1973) and Olsson (2000) in triaxial compression tests of porous sandstone. In analogy to bands of similar orientation, albeit differing deformation mechanism, observed in metals (Nadai, 1950), these authors designated these shallowly inclined bands as Lüders' bands. These authors emphasized the difference between Lüders' bands forming at angles of 37°–55° to the loading direction and without macroscopic shear displacement, and faults with macroscopic shear displacement oriented at ~30° to the loading direction. In these experiments, Lüders' bands formed prior to the formation of faults and failure of the sample. Based on the similar geometric relations between band orientation and shortening direction, we propose that shear-enhanced compaction bands in Aztec Sandstone are analogous to Lüders' bands described by Friedman and Logan (1973) and Olsson (2000) in experiment.

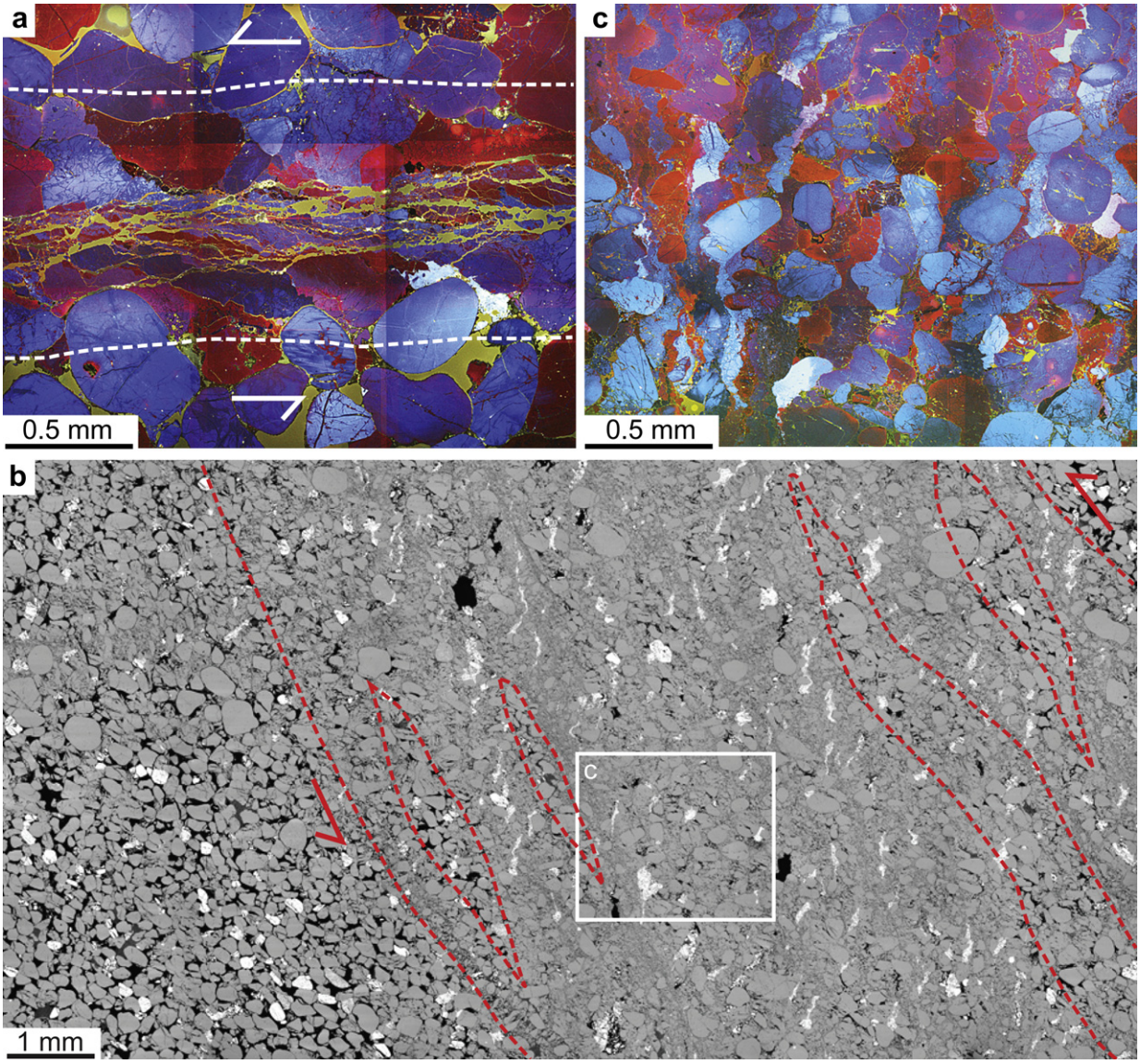

Fig. 11. a. Cathodoluminescence image of a compactive shear band with 2.5 cm of reverse-slip. The band is composed of an outer zone (dashed) of fractured grains and an inner zone of higher grain-size reduction and higher shear strain. b. SEM backscatter of a shear band with 1 cm of slip. The macroscopic band is composed of multiple parallel bands of more intense grain-size reduction. c. Detail of b. imaged with SEM-cathodoluminescence.

Following Olsson (2000), shear-enhanced compaction bands are favored under triaxial loading states ($\sigma_1 > \sigma_2 > \sigma_3$) whereas an axisymmetric loading state ($\sigma_1 > \sigma_2 = \sigma_3$) favors failure along a surface oriented perpendicular to the loading axis. Compaction bands or migrating fronts of localized compaction oriented perpendicular to the loading direction have been obtained in experiment by Olsson (1999); Wong et al. (2001); Haimson and Lee (2004); Tembe et al. (2008), and others. Axisymmetric compression was recently postulated by Issen and Challa (2008) as a condition for the formation of pure compaction bands based on theoretical considerations. The difference between σ_2 and σ_3 is difficult to deduce for the field examples. Yet, given the inclined orientation of σ_1 relative to bedding, and the evidence for bedding-parallel slip in bottom sets, it is reasonable to infer that the differential stress between σ_2 and σ_3 in the more stratified bottom sets would tend to be larger than in the more massive foresets that lack bedding-parallel shear bands. We thus hypothesize that the formation of pure compaction bands is favored in foresets because the differential stress between σ_2 and σ_3 is smaller as compared to the stress state in bottom sets that suppresses the formation of pure compaction bands and favors the formation of shear-enhanced compaction bands and shear bands.

The observed transition from planar to wavy pure compaction bands, chevron-type compaction bands, and ultimately planar shear-enhanced compaction bands along strike of individual bands in foresets may also reflect local changes in stress state that affect the heterogeneity and distribution of the particle flow field in the deforming granular aggregate. The better developed force chains in shear-enhanced compaction bands and the inferred greater coordination in particle movement over larger domains would be favored with increasing differential stress between σ_2 and σ_3, greater grain density (lower porosity), and greater mean stress. The transition from pure compaction to shear-enhanced compaction may thus reflect local variations in stress state and in compaction state of the deforming sand, consistent with Rudnicki (2004) notion that critical conditions for pure compaction and shear band

localization are close for a range of stress states. For shear-enhanced compaction bands, the length scale of domains of coordinated particle flow may control the length of alternating left- and right-lateral chevron-type compaction bands.

4.3. Shear-enhanced compaction bands as distinct structures from compactive shear bands

Shear-enhanced compaction bands are also generally distinct in orientation from compactive shear bands. Where compactive shear bands parallel shear-enhanced compaction bands they either follow bedding planes or existing shear-enhanced compaction bands so that shear bands exploited a pre-existing material anisotropy.

Unlike shear-enhanced compaction bands with slip of ~1 mm or 1/10 of their thickness, shear bands have slip of as much as 2 cm of for a band thickness of 1 mm. Whereas the shear offset along shear-enhanced compaction bands is consistent with shortening oblique to the band orientation, slip on compactive shear bands exceeds the amount that can be attributed to band-oblique shortening. For instance, for a compactive shear band inclined at 32° relative to the shortening direction and assuming band-perpendicular shortening displacement equivalent to a 40% loss in IGV, the band-parallel shear displacement is 1.1 mm. For a band inclined at 7° with an equal amount of porosity loss, the shear displacement is 5.4 mm. These shear displacements are a maximum value assuming an initial porosity of 47%. Significantly smaller shear components would be inferred using the measured differences in IGV inside and outside the band of 4–9% (Table 2) for these calculations. In either case, compactive shear bands accommodate more slip than the amount attributable to band-oblique shortening alone. The comparatively large shear offsets along compactive shear bands are consistent with the microtextural observations of extensive grain-size reduction and slip surfaces, which are both absent from shear-enhanced compaction bands.

Because shear-enhanced compaction bands differ in orientation from compactive shear bands, shear-enhanced compaction bands are generally not precursor structures to shear bands or faults. Although some compactive shear bands are observed to parallel earlier formed shear-enhanced compaction bands where compactive shear bands approach shear-enhanced compaction bands (Fig. 2f, g), compactive shear bands away from shear-enhanced compaction bands do differ in orientation (Figs. 2g and 3). Once shear-enhanced compaction bands reach their compacted state, they are interpreted to strain harden, becoming incapable of accommodating additional shear without a change in stress conditions. Such a change in conditions could be achieved through local or regional rotation of the stress state relative to the stationary band. Except where compactive shear bands parallel shear-enhanced compaction bands, the amount of slip along shear-enhanced compaction bands is thus predetermined by the orientation of the band relative to the loading direction and by the amount of compaction across the band, where the latter is a function of the initial porosity and the stress state. Shear-enhanced compaction bands that have reached their compacted state can accommodate further slip through the formation of closely spaced bands (band multiplication) similar to mechanisms proposed for shear bands (Aydin and Johnson, 1978; Wang et al., 2006), or possibly by outward propagation of the band into uncompacted host rock although field evidence for such band thickening is not observed. In contrast to shear-enhanced compaction bands, compactive shear bands can accommodate comparatively large shear offset commensurate with regional-scale faults through the development of a through-going slip surface (Aydin and Johnson, 1978; Shipton and Cowie, 2003; Davatzes et al., 2005).

This view of shear-enhanced compaction bands as field-geological structures that are distinct from compactive shear bands does not contradict the conceptional framework of a continuous spectrum of band orientations between pure compaction bands to compactive, isochoric, and dilatant shear bands, and to pure dilation bands (Aydin et al., 2006). This framework, and the underlying mathematical theory of deformation localization, relate to the band orientation at the onset of deformation localization but do not consider the subsequent accommodation of finite strain along a band. We interpret the textural and structural differences between shear-enhanced compaction bands and compactive shear bands to reflect differences in post-localization deformation history due to changes in loading conditions and material properties with increasing burial and tectonic loading.

4.4. Evolution of loading conditions and material response at Valley of Fire

Following the constitutive relations of Rudnicki and Olsson (1998); Issen and Rudnicki (2000), and Bésuelle (2001), the orientation of deformation bands in granular media is a function of loading path and the evolving material properties during deformation. Because Aztec Sandstone has changed in its mechanical properties since band formation due to later porosity reduction and diagenesis, present-day laboratory measurements of the constitutive parameters such as the dilatancy factor and hardening modulus would unlikely be representative of Aztec Sandstone at the time of compaction band formation. Nor are established procedures available to derive these parameters from textural and structural information without prior knowledge about the stress state during band formation. A qualitative assessment of the stress state and evolving material properties can be made, however, based on the structural and textural observations within the general framework of critical state theory.

Structural cross-cutting relations indicate that pure and shear-enhanced compaction bands form contemporaneously whereas shear bands generally postdate compaction bands. The change from compaction bands to shear bands likely followed the reduction in porosity and increase in overburden and confining stress. This interpretation is consistent with results from triaxial experiments in Hostun sand at 60 kPa confining pressure, finding a limit or critical porosity of 46% for the formation of compactive shear bands, slightly below the loose packing porosity of 47% (Desrues et al., 1996). While this critical porosity would be lower for a greater confining stress, these results indicate that compaction bands would generally be expected under shallow burial conditions, and probably be limited to loosely packed, well-sorted detrital sediment. Shear bands, on the other hand, are inferred to form in sediment with porosity below the critical porosity. Because shear-enhanced compaction bands are generally unfavorably oriented to evolve into shear bands and macroscopic faults, sediment has to be compacted below the critical porosity before macroscopic faults can form.

The magnitude of the vertical stress at the time of compaction band formation at Valley of Fire can be estimated based on the overburden thickness (Sternlof et al., 2005). The maximum compressive principal stress can then be estimated based on the recognition that compaction band formation was associated with active Sevier thrusting (Hill, 1989; Eichhubl et al., 2004; Eichhubl and Flodin, 2005; Sternlof et al., 2005). We observed clasts of Aztec Sandstone containing deformation bands in conglomerates of the Baseline Sandstone, ~500 m stratigraphically above the top of the Aztec Sandstone (Fig. 1a and b). These clasts indicate that deformation bands formed prior to the exhumation and transport of these clasts, and thus at equal or greater depth than 500 m. With

site B located about 250 m stratigraphically below the top of the Aztec Sandstone we obtain 750 m of overburden at the time of compaction band formation, corresponding to a vertical stress of about 17 MPa for an overburden density of 2250 kg m^{-3}. Based on a structural-diagenetic reconstruction of paleo-fluid flow in the Aztec Sandstone, Eichhubl et al. (2004) concluded that compaction bands formed under fully water-saturated meteoric recharge conditions. With a hydrostatic pressure of 7.5 MPa, the effective vertical stress is ~10 MPa. Assuming that the stress state in this, at the time of band formation, active thrust regime is limited by a Navier-Coulomb failure criterion with a coefficient of internal friction of 0.6 and zero uniaxial compressive strength, and a 26° plunge of the maximum compressive principal stress σ_1, we obtain effective stress magnitudes for σ_1' of 22 MPa, for σ_3' of 7 MPa, and for the effective mean stress of 14.5 MPa. These estimates are about half the stress magnitudes obtained by Sternlof et al. (2005) based a different set of assumptions. Because compaction bands could have formed prior to redeposition of the deformed Aztec Sandstone in the Baseline Sandstone, and thus under less overburden, our calculations may overestimate the stress magnitudes.

4.5. Why are pure compaction bands seemingly uncommon geological structures?

Based on a review of available observations, Issen and Challa (2008) raised the question as to why compaction bands have not been described from more than two locations, Valley of Fire and East Kaibab Monocline, thus far. Our findings suggest that the majority of bands previously described as compaction bands at Valley of Fire are shear-enhanced compaction bands, and that pure compaction bands are even less common than previously thought. We speculate that the relatively large loading stresses conducive to compaction localization are uncommon for sediment above the critical porosity, as they would require a large tectonic stress contribution under very shallow burial conditions. In addition, poor sorting and the abundance of soft grains in compositionally immature sediment could inhibit compaction localization although shear bands in such sediments are not infrequent. The magnitude of the differential stress in active tectonic settings and mechanically layered sediment may provide further limits on the formation of pure compaction bands. Lastly, compaction localization may occur in conjunction with rapid sediment loading in the absence of tectonic loading, producing bedding-parallel compaction bands that are difficult to recognize in outcrop and core. Shear-enhanced compaction bands, on the other hand, may be more common in shallowly deformed sediment. In the past, they may have frequently been misidentified as shear bands in the absence of suitable shear markers and of detailed textural analyses.

5. Conclusions

Based on orientation, structural relations, and microtextural properties we distinguish two types of compaction bands in Aztec Sandstone at Valley of Fire. Pure compaction bands lack any shear component and are inferred to form perpendicular to the loading direction. They are rarely planar but characteristically wavy and tend to transition into a zigzag or chevron geometry. Shear-enhanced compaction bands are interpreted as bands of oblique shortening that accommodate roughly equal band-perpendicular shortening and band-parallel shear displacements, inclined at 38–53° relative to the direction of maximum compressive principal stress. Grain breakage in pure and shear-enhanced compaction bands is largely limited to grain contacts. In shear-enhanced compaction bands, alignments of grains in contact define force chains at ~ 45° to the band orientation. By comparison, compactive shear bands are characterized by macroscopic shear offset >2 cm for a band of 1 mm thickness, the formation of slip surfaces, and greater cataclastic deformation. With the exception of compactive shear bands that reactivate and follow shear-enhanced compaction bands, shear bands form at distinctly smaller angles to the direction of the maximum compressive principal stress. Directions of all bands are fairly uniform across the study area indicative of a homogeneous regional loading state, although it is locally perturbed by bedding plane anisotropy in bottom sets of dune sets.

We infer that the formation of pure compaction bands requires a high initial porosity close to the loose packing porosity, good sorting, near-axisymmetric loading conditions, and effective maximum compressive principal stresses on the order of 20 MPa. Conditions for the formation of shear-enhanced compaction bands may be more relaxed, allowing formation under greater differential stress between σ_2 and σ_3. The requirements for shallow burial and relatively large near-surface tectonic stress contribution may explain the seemingly rare occurrence of tectonic compaction bands. In addition, compaction bands may go unrecognized due to their subtle expression in outcrop and core and a later overprint by continued compaction, cementation, and deformation.

Acknowledgments

This research was partially supported by the Jackson School of Geosciences at the University of Texas, by grant DE-FG02-03ER15430 from Chemical Sciences, Geosciences and Biosciences Division, Office of Basic Energy Sciences, Office of Science, U.S. Department of Energy, and by sponsors of the Fracture Research & Application Consortium. We thank JSG editor Bill Dunne and reviewers John Rudnicki and Haakon Fossen for detailed reviews and suggestions for improvement. Jim Hammons, Park Supervisor of Valley of Fire State Park, and his staff are thanked for their welcome and support of this research.

References

Aschoff, J.L., Schmitt, J.G., 2008. Distinguishing syntectonic unconformity types to enhance analysis of growth strata: an example from the Cretaceous, Southeastern Nevada, USA. Journal of Sedimentary Research 78, 608–623.

Aydin, A., Ahmadov, R., 2009. Bed-parallel compaction bands in aeolian sandstone: their identification, characterization and implications. Tectonophysics 479, 277–284.

Aydin, A., Borja, R.I., Eichhubl, P., 2006. Geological and mathematical framework for failure modes in granular rock. Journal of Structural Geology 28, 83–98.

Aydin, A., Johnson, A.M., 1978. Development of faults as zones of deformation bands and as slip surfaces in sandstone. Pure and Applied Geophysics 116 (4–5), 931–942.

Baud, P., Vajdova, V., Wong, T.-f, 2006. Shear-enhanced compaction and strain localization: inelastic deformation and constitutive modeling of four porous sandstones. Journal of Geophysical Research 111, B12401.

Bésuelle, P., 2001. Compacting and dilating shear bands in porous rock: theoretical and experimental conditions. Journal of Geophysical Research-Solid Earth 106 (B7), 13435–13442.

Bésuelle, P., Rudnicki, J.W., 2004. Localization: shear bands and compaction bands. In: Guéguen, Y., Boutéca, M. (Eds.), Mechanics of Fluid-Saturated Rocks. Elsevier, Amsterdam, pp. 219–321.

Bohannon, R.G., 1977. Geologic map and sections of the Valley of Fire region, North Muddy Mountains, Clark County, Nevada: U.S. Geological Survey Miscellaneous Field Studies Map MF-849.

Borja, R.I., Aydin, A., 2004. Computational modeling of deformation bands in granular media. I. Geological and mathematical framework. Computer Methods in Applied Mechanics and Engineering 193 (27–29), 2667–2698.

Caine, J.S., Evans, J.P., Forster, C.B., 1996. Fault zone architecture and permeability structure. Geology 24, 1025–1028.

Davatzes, N.C., Eichhubl, P., Aydin, A., 2005. Structural evolution of fault zones in sandstone by multiple deformation mechanisms: Moab fault, SE Utah. Geological Society of America Bulletin 117 (1/2), 135–148.

Desrues, J., Chambon, R., Mokni, M., Mazerolle, F., 1996. Void ratio evolution inside shear bands in triaxial sand specimens studied by computed tomography. Geotechnique 46 (3), 529–546.

Du Bernard, X., Eichhubl, P., Aydin, A., 2002. Dilation bands: a new form of localized failure in granular media. Geophysical Research Letters 29 (24), 2176.

Eichhubl, P., 2007. Two types of compaction Bands in Aztec Sandstone at Valley of Fire, NV. Eos Transactions AGU 88 (52) Fall Meeting Supplement, Abstract T43E-02.
Eichhubl, P., Flodin, E., 2005. Brittle deformation, fluid flow, and diagenesis in sandstone at Valley of Fire State Park, Nevada. In: Pederson, J., Dehler, C.M. (Eds.), Interior Western United States. Geological Society of America Field Guides 6, pp. 151–167.
Eichhubl, P., Taylor, W.L., Pollard, D.D., Aydin, A., 2004. Paleo-fluid flow and deformation in the Aztec Sandstone at the Valley of Fire, Nevada-evidence for the coupling of hydrogeologic, diagenetic, and tectonic processes. Geological Society of America Bulletin 116, 1120–1136.
Fortin, J., Stanchits, S., Dresen, G., Guéguen, Y., 2006. Acoustic emission and velocities associated with the formation of compaction bands in sandstone. Journal of Geophysical Research 111, B10203.
Fossen, H., Schultz, R.A., Shipton, Z.K., Mair, K., 2007. Deformation bands in sandstone: a review. Journal of the Geological Society London 164, 755–769.
Friedman, M., Logan, J.M., 1973. Lüders' bands in experimentally deformed sandstone and limestone. Geological Society of America Bulletin 84, 1465–1476.
Haimson, B., Lee, H., 2004. Borehole breakouts and compaction bands in two high-porosity sandstones. International Journal of Rock Mechanics and Mining Sciences 41 (2), 287–301.
Hill, R.E., 1989. Analysis of Deformation Bands in the Aztec Sandstone, Valley of Fire State Park, Nevada. M.S. thesis. University of Nevada, Las Vegas, 68 p.
Holcomb, D., Rudnicki, J., Issen, K., Sternlof, K., 2007. Compaction localization in the earth and the laboratory: state of the research and research directions. Acta Geotechnica 2 (1), 1–15.
Houlsby, G.T., Wroth, C.P., 1980. Strain and displacement discontinuities in soil. Journal of the Engineering Mechanics Division 106, 753–771.
Issen, K.A., Challa, V., 2008. Influence of the intermediate principal stress on the strain localization mode in porous sandstone. Journal of Geophysical Research 113, B02103. doi:10.1029/2005JB004008.
Issen, K.A., Rudnicki, J.W., 2000. Conditions for compaction bands in porous rock. Journal of Geophysical Research 105 (B9), 21529–21536.
Marzolf, J.E., 1990. Reconstruction of extensionally dismembered early Mesozoic sedimentary basins; Southwestern Colorado Plateau to the eastern Mojave Desert. In: Wernicke, B.P. (Ed.), Basin and Range Extensional Tectonics Near the Latitude of Las Vegas, Nevada. Geological Society of America Memoir 176, pp. 477–500.
Mollema, P.N., Antonellini, M.A., 1996. Compaction bands: a structural analog for anti-mode I cracks in aeolian sandstone. Tectonophysics 267, 209–228.
Nadai, A., 1950. Theory of Flow and Fracture of Solids. McGraw-Hill, New York.
Oda, M., Konishi, J., Nemat-Nasser, S., 1982. Experimental micromechanical evaluation of strength of granular materials: effects of particle rolling. Mechanics of Materials 1 (4), 269–283.
Olsson, W.A., 1999. Theoretical and experimental investigation of compaction bands in porous rock. Journal of Geophysical Research-Solid Earth 104 (B4), 7219–7228.
Olsson, W.A., 2000. Origin of Lüders' bands in deformed rock. Journal of Geophysical Research-Solid Earth 105 (B3), 5931–5938.
Potyondy, D.O., Cundall, P.A., 2004. A bonded-particle model for rock. International Journal of Rock Mechanics and Mining Sciences 41 (8), 1329–1364.
Rudnicki, J.W., 2004. Shear and compaction band formation on an elliptic yield cap. Journal of Geophysical Research 109, B03402.
Rudnicki, J.W., Olsson, W.A., 1998. Reexamination of fault angles predicted by shear localization theory. International Journal of Rock Mechanics and Mining Sciences 35, 512–513.
Schultz, R.A., 2009. Scaling and paleodepth of compaction bands, Nevada and Utah. Journal of Geophysical Research 114, B03407. doi:10.1029/2008JB005876.
Shipton, Z.K., Cowie, P.A., 2003. A conceptual model for the origin of fault damage zone structures in high-porosity sandstone. Journal of Structural Geology 25 (3), 333–344.
Sternlof, K.R., Chapin, J.R., Pollard, D.D., Durlofsky, L.J., 2004. Permeability effects of deformation band arrays in sandstone. AAPG Bulletin 88, 1315–1329.
Sternlof, K.R., Rudnicki, J.W., Pollard, D.D., 2005. Anticrack inclusion model for compaction bands in sandstone. Journal of Geophysical Research-Solid Earth 110 (B11).
Tembe, S., Baud, P., Wong, T.-f, 2008. Stress conditions for the propagation of discrete compaction bands in porous sandstone. Journal of Geophysical Research 113, B09409. doi:10.1029/2007JB005439.
Wang, G., Liu, Y.H., Yu, P., Zhao, D.Q., Pan, M.X., Wang, W.H., 2006. Structural evolution in TiCu-based bulk metallic glass with large compressive plasticity. Applied Physics Letters 89 (25), 3.
Wong, T.-f., Baud, P., Klein, E., 2001. Localized failure modes in a compactant porous rock. Geophysical Research Letters 28 (13), 2521–2524.